NJC

ROYAL SOCIETY OF CHEMISTRY

PAPER

View Article Online
View Journal

Cite this: DOI: 10.1039/d0nj04431h

Non-enzymatic electrochemical glucose sensing by Cu_2O octahedrons: elucidating the protein adsorption signature†

Soumyadipta Rakshit, [a] Srabanti Ghosh, [b] Rimi Roy[c] and Subhash Chandra Bhattacharya *[a]

Received 3rd September 2020,
Accepted 30th November 2020

DOI: 10.1039/d0nj04431h

rsc.li/njc

A facile solution based chemical route has been developed for the synthesis of cuprous oxide (Cu_2O) octahedrons employing polyvinylpyrrolidone (PVP ~ 10k) at a relatively low temperature (50 °C) in aqueous medium and their response towards electrochemical non-enzymatic glucose sensing has been precisely investigated. The amperometric analysis reveals two calibration ranges (0.1 μM–1 mM and 1–7 mM) for the modified electrodes, with an excellent glucose specific selectivity over other interfering materials like sucrose, fructose, ascorbic acid (AA) and dopamine (DA). Careful analysis of the amperometric outcomes unveils a low limit of detection (LOD) of 0.96 μM (S/N = 3) along with exceptionally good stability and repeatability. Furthermore, the octahedral Cu_2O modified electrodes exhibit a fast response time (~1.5 s) with acceptable sensitivity and are found to be exceedingly reliable for the real time analysis of human serum samples (relative error <3.2%) compared to commercial glucose biosensors. Detailed survey of the adsorption of four most common blood proteins onto the negatively charged surface of Cu_2O octahedrons using steady state fluorescence, dynamic light scattering (DLS), zeta potential (ζ) and circular dichroism (CD) in aqueous dispersions delineates the electrostatic interaction driven low protein adsorption that strongly indicates their further potential applicability in medical devices for targeted monitoring of glucose.

1. Introduction

Diabetes poses an immediate threat to innumerable human lives and in order to overcome this threat, the regular monitoring of physiological glucose levels is essential. Although research on glucose sensors began decades ago, this particular field still draws immense interest because of their versatility and potential for commercial return. Apart from clinical diagnosis, effective and precise means of determining glucose levels have received vital attention in food analysis, brewing, and biotechnology.[1–5] Therefore, the development of a highly-sensitive, repetitive and inexpensive sensing tool for the detection of glucose is an urgent challenge to meet, under current circumstances. Amongst several methods available to date for the real-time monitoring of glucose concentration, amperometric enzymatic glucose sensors based on glucose oxidase have played a pivotal role owing to their sensitivity, efficiency, precision, response time and simple operation.[6] However, the stability of the enzyme based amperometric sensors can be easily influenced by pH, humidity, toxic materials, and altered temperature; due to the intrinsic nature of enzymes and the complexity of the enzyme immobilization process.[7,8] As a result of the inherent frailty of the enzymes, nonenzymatic glucose sensors centred on the electrocatalytic oxidation of glucose by a variety of electrocatalysts have come to the limelight as an alternative. However, numerous nonenzymatic sensors exhibit low sensitivity and poor selectivity as a result of the surface poisoning arising from different adsorbed intermediates and chloride.[9] In this regard, metal oxide based nonenzymatic glucose sensors have offered marked efficacy in terms of high electrocatalytic activity, low cost, and decent stability.[6,10]

Cu_2O, a cubic semiconductor material with a = 4.27 Å and $Pn3m$ symmetry, has been deliberately explored over the years by researchers due to its basic condensed matter physics studies including the observation of Bose–Einstein condensation of excitons.[11,12] Moreover, Cu_2O has a large absorption coefficient that ranges from the violet to green solar spectrum which is highly efficient in solar cells and photodiodes, for the conversion of solar energy to electrical or chemical energy.[13,14] Its non-toxic nature and high abundance in the earth's crust have made Cu_2O a suitable candidate to be extensively

[a] Department of Chemistry, Jadavpur University, Kolkata 700 032, India. E-mail: sbjuchem@yahoo.com
[b] Department of Chemical, Biological and Macromolecular Sciences, S. N. Bose National Centre for Basic Sciences, Block JD, Sector III, Salt Lake, Kolkata 700 098, India
[c] Department of Chemistry, Presidency University, Kolkata 700 073, India

† Electronic supplementary information (ESI) available. See DOI: 10.1039/d0nj04431h

exploited in diverse fields, such as photocatalysis,[15] gas sensors,[16] non-enzymatic glucose and peroxide sensors,[17,18] organic reaction catalysis,[19,20] water splitting[21] and electrode materials.[22] In addition, usage of Cu_2O benefits from its low oxidation potential in alkaline solutions that consequently leads to enhanced sensitivities compared to other metal oxides. Cu_2O micro/nanocrystals have been utilized extensively for their promising electrocatalytic activity over recent years.[23–25] However, a majority of the reports on the electrochemical sensing of glucose dealing with pure Cu_2O usually lack in sensitivity and display a poor linear range. In recent times, Cu_2O based composites[26–28] have been applied to biosensors to assess their response performance, but, still there exists ample scope to augment the electrocatalytic activity of pure Cu_2O itself and our present work contributes towards this aim.

Well organized nano/microstructures with apposite size, morphology and arrangement have long been a focus of research owing to their enhanced properties and potential usage in numerous fields, for instance, catalysis, biosensors, nanoelectronics, and energy harvesting.[29–31] To exploit the structure–morphology–activity relationship of various microstructures, morphology control has garnered lots of attention in fundamental research as well as in technical applications. The underlying motive is to discover unique nano/microscale structures with improved properties.[32,33] A normal surfactant templating method for quick and gram scale synthesis of oxide materials often results in disoriented structures with high polydispersity due to inappropriate geometry and molecular orientation or an inability to sufficiently lower the interfacial tension between the two fluids.[34,35] But, PVP can serve as a surface stabilizer, growth modifier, nanoparticle dispersant, and as a reducing agent. The key advantage of using PVP lies in its solubility in aqueous and many non-aqueous solvents because of the presence of a strong hydrophilic pyrrolidone moiety together with a considerable hydrophobic alkyl group. The roles that PVP adopts depend entirely on the specific material class, reaction conditions, and even the PVP itself on account of the availability of different molecular weights.[36] PVP with different molecular weights ($\sim$55k, $\sim$40k, $\sim$30k) has commonly been employed in the preparation of Cu_2O spheres, rods and cubes.[37–39] Yet, the octahedral structure of Cu_2O has never been achieved using PVP and our current work outlines the first time use of PVP-10k (M.W. $\sim$ 10 000) in the construction of octahedral Cu_2O.

In electrochemical sensing devices, the effective electroactive surface area is negligible compared to the overall surface area of the device itself. The miniatured biosensors used by the medical fraternity are generally made using thick-film screen printing and/or thin-film photolithography.[40,41] Although these single use biochips/assays have the ability towards acute detection and measurement of biomolecules by using a few microlitres of samples, biofouling alone does not allow these chips to gain the necessary popularity. In the field of electrochemical glucose biosensors, electrode fouling due to non-specific protein adsorption is an actual threat, and the utmost vital concern in designing efficient electrochemical biosensors is the immobilization of proteins.[42–44] Lately, increasing research on the design of electrochemical bio and immunosensors and analytical devices makes the issue relevant.[45,46] Since proteins contain hydrophobic and hydrophilic domains with positive and negative charges, their interactions with different surfaces are ubiquitous which has been proved to be a key parameter to assess the functionality of the materials towards real time analysis of samples. Comprehension of the protein adsorption on the surface of materials can provide a pertinent way to understand their analytical performance as well.[47,48] Our present work preferentially outlines the phenomena of non-specific protein adsorption onto the surface of Cu_2O octahedrons to unveil their future applicability towards analytical device fabrication.

In this present contribution, we report a low-cost, and environmentally benign approach for the gram-scale synthesis of uniform octahedral Cu_2O microstructures. PVP-10k (M.W. $\sim$ 10 000) is employed as the stabilizer and ascorbic acid serves the role of a potent reducing agent. Detailed structural characterization is carried out by means of XRD, FESEM and TEM analyses. Systematic electrochemical properties of the as prepared hierarchical Cu_2O microstructures reveal their low detection limit, fast response, and fairly high sensitivity towards non-enzymatic glucose detection. Their successful application towards determining the glucose level in real blood samples offers great potential in the field of electrochemical biosensor devices. Regarding the application in real biological samples, the four most common blood proteins namely, human serum albumin (HSA), γ-globulin (γ-GB), fibrinogen (Fib), and hemoglobin (Hb) have been chosen to realize how the proteins are absorbed on the surface of the Cu_2O octahedrons to form a new interface with a compact "biological identity". To gain insights into the protein adsorption phenomena, steady state fluorescence, circular dichroism, and DLS experiments are conducted under physiological conditions (pH $\sim$ 7.2). The smooth surfaced and negatively charged Cu_2O octahedrons turn out to be less prone towards protein adsorption. However, their adsorptivity towards fibrinogen is comparatively higher in comparison to the other studied proteins. These outcomes demonstrate the low electrostatic interaction between the Cu_2O and the studied proteins, resulting in a more biologically active material for real time applications.

2. Experimental

2.1. Chemicals

The precursor metal salt cupric acetate ($Cu(OAc)_2$), polyvinylpyrrolidone-10k, ascorbic acid, Nafion, Na_2HPO_4, NaH_2PO_4 and blood proteins (HSA, Fib, Hb and γ-GB) were purchased from Aldrich and Merck. All reagents were used as received without further purification from the commercial suppliers unless otherwise noted. The water used was treated using a Millipore-Q water purification system. Human serum samples were obtained from Serobacto Pathological Laboratory.

2.2. Synthesis of Cu_2O octahedrons

In a typical experiment, 0.2 g of PVP (M.W. $\sim$ 10 000) was dissolved in 18.6 mL of water and the solution was stirred until it attained homogeneity. Next, 0.2 mL of 0.2 M $Cu(OAc)_2$

solution was added to it and the resulting solution was stirred at 50 °C for two and a half hours. To this solution, 0.2 mL of 1 M NaOH solution was added dropwise, which resulted in an immediate colour change of the solution to blackish brown. After 5 min of stirring, 1 mL of 0.5 M ascorbic acid was poured into the mixture and the solution turned a reddish color instantaneously, indicating the initiation of the reduction process to form Cu_2O. The final mixture was stirred for another 30 min at 50 °C and subsequently cooled down to room temperature. The resulting precipitate was collected by centrifugation (8000 rpm), washed with distilled water and ethanol, and dried under vacuum for 8 hours at 40 °C.

2.3. Preparation of the Cu_2O modified electrode

Fabrication of the Cu_2O modified electrode was done using the following method: a glassy carbon electrode (GCE) was first polished and successively washed with water and ethanol several times. A diluted Nafion solution (0.025% v/v) was prepared by adding 0.7 mL water and 0.3 mL isopropanol to a 5 mL Nafion solution. Next, 2 mg of the earlier prepared Cu_2O sample was dispersed in 1 mL of the diluted Nafion solution, and this was subjected to ultrasonication for 2 hours. At last, 20 μL of the corresponding suspension (2 mg mL^{-1}) was cast on the GCE surface and dried in air (25 °C). The electroactive surface area of the GCE was found to be 0.11 mm^2.

2.4. Apparatus and measurements

Crystal phase analysis of the synthesized cuprous oxide was performed using an X-ray diffractometer with Cu-Kα radiation (λ = 0.15406 nm) in a 2θ angular range of 20°–80° at a scanning speed of 2° min^{-1}. The surface morphology of the Cu_2O microstructures was examined using field emission scanning electron microscopy (FESEM, Hitachi S-4800, Japan) and high-resolution transmission electron microscopy (HRTEM, JEOL-JEM-2100) at an accelerating voltage of 200 kV.

Amperometric and cyclic voltammetry (CV) experiments were executed using a CHI 650E electrochemical analyzer (CHI, USA) with a conventional three-electrode cell. The working electrode was a modified glassy carbon electrode. Ag/AgCl and a platinum wire were used as the reference and auxiliary electrodes, respectively. 0.1 M NaOH solution was employed as the supporting electrolyte. The effective surface area was estimated using cyclic voltammetry in 0.1 M KCl solution containing 1 mM $K_3Fe(CN)_6$ at various scan rates. The electrolytic solutions were purged with purified nitrogen for at least 30 min before electrochemical measurements. All the experiments were carried out at room temperature.

2.5. Protein adsorption study

2.5.1. Procedure. To determine the protein adsorption onto the surface of Cu_2O octahedrons, at first, 2.5 mg of the synthesized material was dispersed in 4.5 mL of phosphate buffer (PBS; pH ~ 7.2 ± 0.2) for 30 min at a fixed temperature of 25 °C and then 0.5 mL of a 2 mg mL^{-1} protein solution was added to the previous solution containing the material. The resultant mixture was stirred gently at a temperature of 4 °C for 6 hours. The material was then centrifuged at 1000 rpm for 25 min at 4 °C. The concentrations of the proteins in the supernatants were measured by determining the emission maxima using steady state fluorescence spectroscopy (Shimadzu spectrofluorimeter; model: RF5301, equipped with a quartz cell of path length 10 mm). A calibration curve for each of the proteins was prepared using the intensity of the emission maxima at different concentrations of the concerned protein. The amount of protein adsorbed was estimated using the following equation:

$$A = \frac{(C_p - C_s) \times V}{m}$$

where A is the amount of protein adsorbed, C_p and C_s are the corresponding protein concentrations at the initial state and in the supernatant after adsorption studies. V represents the total volume of the solution (5 mL) and m denotes the weight of Cu_2O added into the solutions.

2.5.2. DLS and zeta potential measurements. Hydrodynamic radius and zeta potential of the synthesized octahedrons, proteins and protein adsorbed microstructures were recorded using a Zetasizer (Nano-ZS) from Malvern Instruments.

2.5.3. Circular dichroism (CD) study. CD spectra of the proteins before adsorption and in the supernatant after adsorption were evaluated using a JASCO, CD Spectrometer; model: J-815-15OS using a 0.1 cm path length quartz cell in a wavelength range between 180 and 350 nm. The raw data were then deconvoluted and analyzed using CDNN software.

3. Results and discussion

3.1. Structural characterization of the as synthesized Cu_2O microstructures

At the outset, the crystallinity and phase composition of the as synthesized microstructured Cu_2O were explored using powder X-ray diffraction (XRD) analysis (Fig. 1a). In accordance with the XRD data, the corresponding six peaks with 2θ values of 29.62, 36.46, 42.34, 61.41, 73.54 and 77.42 can be successfully assigned to the 110, 111, 200, 220, 311 and 222 planes of Cu_2O. All the diffraction peaks can readily be indexed to cubic phase Cu_2O

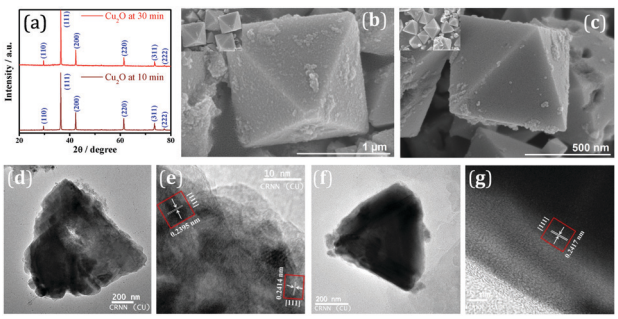

Fig. 1 (a) X-Ray diffraction pattern of the Cu_2O octahedrons at 10 and 30 min reaction time intervals. (b) and (c) Illustrates the FESEM images of the Cu_2O octahedrons fabricated at 10 and 30 min. The inset shows their corresponding distribution. (d–g) The corresponding TEM and HRTEM images of the as synthesized Cu_2O microstructures collected at 10 and 30 min reaction time intervals.

(space group: $Pn\bar{3}m$, a = 0.4294 nm) with no impurity (JCPDS no. 75-1531).[49] The appearance of strong and narrow diffraction peaks signifies the crystalline nature of the products. It is known that the facets with a slower growth rate would be more exposed on the crystal surface and consequently exhibit a relatively stronger diffraction intensity in the corresponding XRD patterns.[39] From the XRD, the diffraction peak of the (111) plane is found to be the strongest. The ratio between the intensities of the two strongest peaks is indicative of the preferential growth of a material. The ratio of the (111) and (200) planes at a reaction time of 10 min is found to be 3.05 which increases up to 3.4 after the completion of the reaction (30 min). The higher value of the ratio in comparison to the standard value of 2.70 at both the time scales substantiates preferential growth along the (111) plane.[49,50]

After ascertaining the synthesis of a chemically pure phase Cu_2O, FESEM is carried out to visualize the morphology and the structural patterns of the as synthesized products. Fig. 1b and c illustrate the FESEM images of the as synthesized Cu_2O. The microstructures exhibit the typical octahedral morphology with a mean edge length of 1.2 ± 0.1 μm at the reaction time of 10 min. The structures are then penetrated using a reducing agent in a symmetric fashion with time to produce smaller Cu_2O octahedrons with an average size of 500 nm with a standard deviation of 50 nm. Correspondingly, higher magnification reveals the smooth surface of the Cu_2O octahedrons as well.

The hierarchical structures of Cu_2O are further elucidated using transmission electron microscopy (TEM) which reinforces the above observation. Fig. 1d and f demonstrate the typical TEM images of Cu_2O microstructures obtained at 10 and 30 min, whereas Fig. 1e and g denote the most prominent lattice plane present and have been indexed and correspond to the (111) plane obtained from careful HRTEM observation, which is consistent with our XRD results. The lattice fringes in the HRTEM images are distinguished using white lines and arrows, and the corresponding lattice spacing in each case is in good agreement with the d value of the (111) facets of the Cu_2O crystal (0.2440 nm). The preliminary growth direction of the (111) facets follows a heterogeneous manner indeed; but, with time it becomes homogeneous. This observation is in line with the results of the XRD analysis.

It has been established that the construction of Cu_2O microstructures goes through the formation of $Cu(OH)_2$ in the first step and $[Cu(OH)_4]^{2-}$ in the second, which subsequently get reduced by the reducing agent.[51] Since our method resulted in a proper shape, it might be presumed that the complex covered with the stabilizing agent PVP, at first, gets adsorbed on the building blocks of Cu_2O microstructures, to direct preferential growth along a particular facet, generating the octahedral shape. However, from a thermodynamic point of view it is quite evident that in order to minimize the overall energy of the total system, the building blocks tend to aggregate into a particular shape or architecture. To thoroughly comprehend the formation and growth mechanism, we attempted time-dependent FESEM, TEM and HRTEM analyses. The FESEM and TEM (Fig. S1, ESI†) images of the Cu_2O microstructures at different time intervals corroborate the fact that the synergic effect of the nanoparticle aggregation and ripening mechanism leads to facet-selective adsorption to affect morphological evolution. Homogeneous growth along the (111) facet is observed with reaction time. In the beginning, we encounter the octahedral structure for Cu_2O, but with time it becomes smaller in dimension and retains the original shape. In general, a prolonged reaction time causes aggregation to produce bulkier and improper structures. However, in this case, the reducing agent further attacks the octahedrons to produce smaller shaped Cu_2O rather than inducing ripening (Fig. S1, ESI†). PVP-10k, in effect, plays a crucial role in the second step after Cu_2O attains a proper shape. PVP is normally used as a stabilizer to impede nanoparticle aggregation. It is seen that PVP comprising of a shorter chain length fails to provide stability to the formed microstructures.[36] In our case, it can be assumed that due to the reduced stability of PVP-10k, the bigger octahedrons are not in thermodynamic equilibrium and become metastable to enhance the surface area by forming octahedrons of shorter dimensions.

3.2. Electrochemical behavior

3.2.1. Cyclic voltammetry study of the bipyramidal Cu_2O modified electrode towards glucose. The electrochemical response of the octahedral Cu_2O modified GCE has been studied using cyclic voltammetry (CV). Fig. 2 systematically presents the typical cyclic voltammograms of the bare GCE, octahedral Cu_2O modified GCE in 0.1 M NaOH with and without the presence of glucose at 100 mV s^{-1}. No noticeable electrochemical redox peaks are observed when CVs are performed on bare GCE (Fig. 2a, black line). However, a pair of well-defined redox peaks are observed to be generated after the inclusion of the octahedral Cu_2O modified electrode (Fig. 2a, red graph).

This can be ascribed to the involvement of Cu(II) and Cu(III) surface species. Moreover, the distinct electrochemical signal of the Cu_2O modified electrode compared to that of bare GCE (Fig. 2a, red graph) suggests that the former electrode is highly suitable for electrochemical detection. Fig. 2b displays an obvious increase in the reduction peak intensity due to the addition of 0.05 mM glucose into the 0.1 M NaOH solution. The reduction peak escalates rapidly with further increase in

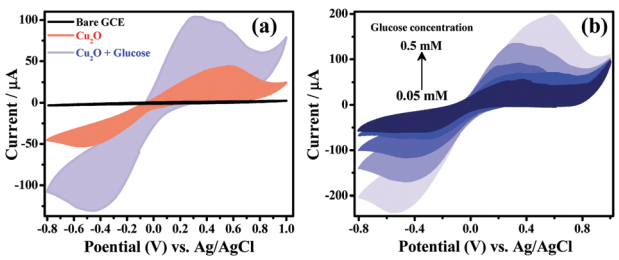

Fig. 2 (a) Cyclic voltammograms (CVs) of the as synthesized Cu_2O octahedron modified GCE in 0.1 M NaOH solution with (blue graph) and without 0.25 mM glucose (red graph). The black line indicates the CV obtained for the bare GCE electrode in 0.1 M NaOH in the presence of 0.25 mM glucose for comparison. (b) CVs of the Cu_2O electrode in a 0.1 M NaOH solution containing different concentrations of glucose. A scan rate of 50 mV s^{-1} is used for the above experiments.

the concentration of glucose to 0.5 mM. Hence, the above experimental observation is sufficient to substantiate the electrocatalytic activity of the octahedral Cu_2O modified electrode towards glucose.[52,53] Within the potential range of 0.3–0.8 V, glucose is oxidized to gluconolactone which primarily corresponds to the Cu^{2+}/Cu^{3+} conversion. In this high potential range, a catalytic species, Cu^{3+} gets formed at the surface of the Cu_2O modified electrode and is believed to be an electron transmitter.[54] Although the underlying mechanism of glucose oxidation over the Cu_2O surface is unclear, it is to be believed that the species Cu(III) is more accountable towards the facilitation of electron transfer than Cu(I) and Cu(II).[24] The plausible mechanism of glucose oxidation at the surface of the Cu_2O octahedrons is summarized in Scheme 1.[24,25]

3.2.2. Effect of scan rate. The effect of scan rate on the voltammetric behavior of glucose oxidation has also been investigated. Fig. 3a shows the CVs of the as synthesized Cu_2O modified electrode in 0.1 M NaOH at different scan rates ranging from 20 to 150 mV s^{-1}. As illustrated in Fig. 3b, both the cathodic and anodic peak currents increase gradually upon increasing the scan rates. However, the peak potentials shift to opposite directions, *i.e.*, negatively for the cathodic peak and positively for the anodic peak, which further confirms that the kinetics of the overall process is predominantly controlled by the diffusion process. The regression equations are expressed as below

$$I_{pa} = -0.6589\nu^{1/2} + 1.5871\ (\mu A, \text{mV s}^{-1}, R^2 = 0.998)$$

and

$$I_{pc} = 0.5494\nu^{1/2} - 0.3282\ (\mu A, \text{mV s}^{-1}, R^2 = 0.999)$$

The relationship between the peak potentials (E_{pa}) and the logarithm of scan rate ($\log \nu$) is portrayed in Fig. 3c. Two respective straight lines are generated with the slopes of $-2.303RT/\alpha nF$ and $2.303RT/(1-\alpha)nF$ for the cathodic and anodic peaks, where α is the electron transfer coefficient, n is the number of exchange

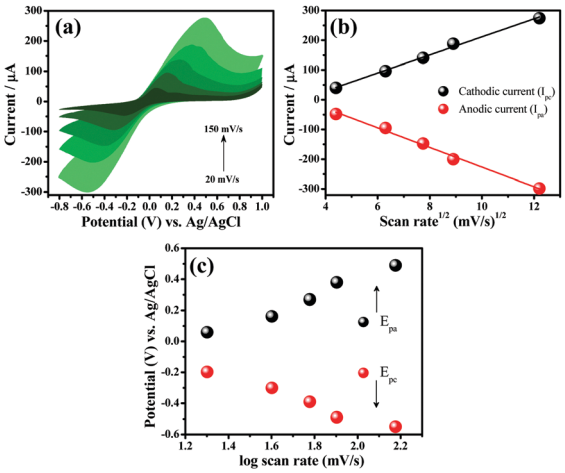

Fig. 3 (a) Cyclic voltammograms of the bipyramidal Cu_2O modified electrode in deoxygenized 0.1 M NaOH at various scan rates (20–150 mV s^{-1}). (b) Plots of anodic and cathodic peak currents *versus* the square root of the scan rate. (c) Dependence of anodic and cathodic peak potentials *versus* the logarithm of the scan rate.

electrons (n = 1), and R, T, and F bear their usual meaning. Two linear regression equations

$$E_{pa} = 0.02906 \log \nu + 0.01722\ (\text{V, mV s}^{-1}, R^2 = 0.996)$$

and $E_{pc} = 0.08674 \log \nu + 0.03528$ (V, mV s^{-1}, R^2 = 0.989) can be obtained corresponding to the anodic and cathodic peak potentials, respectively. The estimated value is found to be 0.65 from the slopes of the straight lines using the following equation:[55]

$$\frac{\nu_a}{\nu_c} = \frac{\alpha}{\alpha - 1}$$

where ν_a and ν_c are determined by the x-intercepts of the lines for the anodic and cathodic branches, respectively. The minimum value of α should be 0.5 for all standard reaction mechanisms.[55,56] Therefore, values greater than 0.5 indicate the feasibility of the reaction which also reinforces the favoured electrocatalytic reduction of glucose on the octahedral Cu_2O modified electrode compared to the bare glassy carbon electrode.

3.2.3. Amperometric response of glucose on the octahedral Cu_2O modified electrode. The steady state amperometric response of the octahedral Cu_2O modified electrode with successive additions of glucose into 5 mL of 0.1 M NaOH solution at an applied potential of 0.6 V is presented in Fig. 4a. A fast and sensitive response of the modified electrode towards glucose can be clearly witnessed. Careful analysis of Fig. 4a reveals that the response time is 1.45 s (Fig. S2, ESI†). Fig. 4b displays an upsurge of amperometric current on increasing the glucose concentration. Two different linear ranges have been obtained. The first calibration curve shows a linear response from 0.1 μM to 1 mM (Fig. 4b and Fig. S3, ESI†) and by using the linear regression equation and electroactive surface area[57,58] the sensitivity of the modified electrode is found to be 382.98 μA mM^{-1} cm^{-2} for this concentration range. Whereas from the other calibration curve at a higher concentration range (1–7 mM), the sensitivity is found to be 55.59 μA mM^{-1} cm^{-2}. The lesser value for sensitivity at a higher

(1) $Cu^{1+} + OH^- \rightarrow Cu^{2+} + e^-$

(2) $Cu^{2+} + OH^- \rightarrow Cu^{3+} + e^-$

(3) $Cu^{3+} + Glucose + e^- \rightarrow Cu^{2+} + gluconolactone + OH^-$

(4) $Cu^{2+} + Glucose + e^- \rightarrow Cu^{1+} + gluconolactone + OH^-$

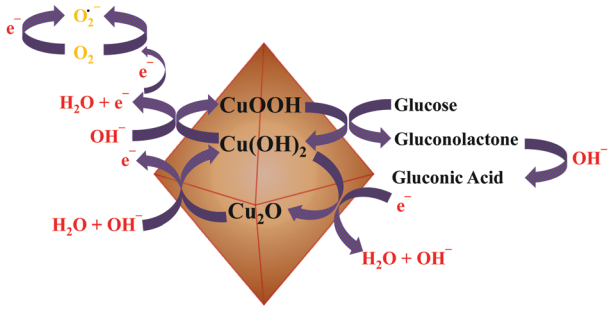

Scheme 1 Depiction of a plausible mechanism of glucose oxidation at the surface of Cu_2O octahedrons.

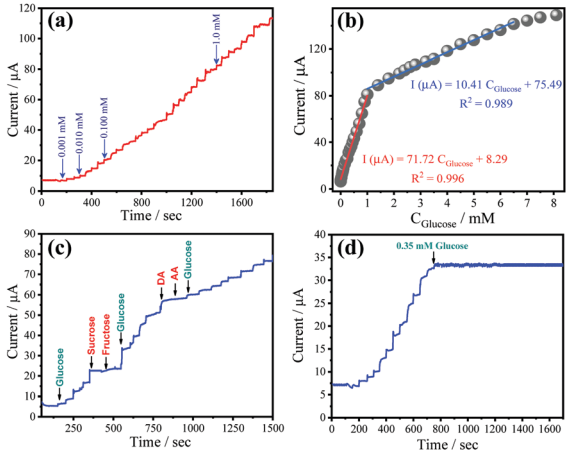

Fig. 4 (a) Amperometric responses of the Cu_2O modified electrode after successive injections of glucose (the amount is indicated by arrows in the plot) in 0.1 M NaOH at 0.60 V. (b) Dependence of current at 0.6 V on glucose concentration. (c) Response of various interferons added to glucose at 0.60 V. (d) Amperometric response of the electrode upon the addition of 0.35 mM glucose during 1600 s.

concentration can be ascribed to the saturation of the electrode surface and the lower abundance of active sites that result in a lower slope value.[57] We have calculated the limit of detection (LOD) from the slope of the plot of ΔI *vs.* $C_{glucose}$ (Fig. S4, ESI†). The linear regression equation can be written in the form

$$\Delta I\ (\mu A) = 1.607 \log C_{glucose}\ (mM) + 5.115\ (R^2 = 0.951)$$

LOD was calculated according to the equation DL = 3*S*/*N*, where *S* is the slope of the calibration curve and *N* is the standard deviation of the blank measurements ($N = 5$).[59,60] LOD was found to be 0.96 μM. The above depicted results therefore unveil the admirable electrocatalytic performance of the octahedral Cu_2O modified electrode along with a fast response time, low detection limit and relatively high sensitivity. The stability of the as synthesized octahedral Cu_2O modified electrode has been measured by determining its residual current response to 1 mM glucose (Fig. 4b). 95.1% of the initial value of the peak current of the Cu_2O modified electrode is retained after storing at 4 °C for a week, and even after three weeks, the peak current response is found to keep 85.3% of its initial value. These can be attributed to the presence of a Nafion membrane and the unique octahedral structure of Cu_2O that may have contributed towards the long-term stability of the modified electrode.

In human blood apart from glucose, several other oxidation species are also present and it is essential to distinguish these interferons. D-Fructose and sucrose display similar electrical responses to glucose, and ascorbic acid (AA) and dopamine (DA) also interfere in the accurate detection of glucose. So, inspecting the selectivity of a non-enzymatic glucose sensor preferentially determines its applicability towards real sample measurement. In human blood, the corresponding ratios of DA and AA to glucose is 1 : 13 and 1 : 69.[61] Therefore, both the elements have been added at a ratio of 1 : 10 to glucose which is higher than their corresponding concentrations under physiological conditions in real blood samples. Fig. 4c demonstrates the amperometric response of the Cu_2O octahedron modified electrode upon the addition of 0.1 mM of the above-mentioned interferons along with 1.0 mM glucose at different time periods. The current responses of the interfering agents are negligible compared to the response caused by the addition of glucose. The strong amperometric signal of the Cu_2O modified electrode in the presence of different interferons establishes excellent selectivity and specificity towards glucose sensing. The low working potential and the use of negatively charged Nafion might be the reasons for repelling the interfering substances such as ascorbic acid and dopamine easily.[55] Fig. 4d shows the amperometric response of the Cu_2O modified electrode upon the addition of 0.35 mM glucose during 1600 s, suggesting high stability with a constant current response.

It can be presumed that the unique architecture and over-exposed (111) plane of the octahedrons may be responsible for the superior response towards glucose. The key performance characteristics of the as prepared Cu_2O octahedron catalyst are compared with some of the existing nonenzymatic glucose sensors derived from Cu_2O, as listed in Table ST1 (ESI†) and the outcomes undoubtedly show competitive and comparable results with other reported Cu_2O based glucose sensors in terms of sensitivity, selectivity, response time and linear calibration range.

3.2.4. Application of the glucose biosensor to real samples. In order to evaluate the real time practical applications of the proposed biosensor, glucose concentration in a variety of serum samples was assayed. The serum samples were provided as a gift by Serobacto Pathological Laboratory to be used for academic purposes only. The serum samples were first analyzed in the Pathological Laboratory using a MISPA NEO Biochemistry Analyzer system. These samples are diluted ten times with water and then directly applied for the detection of glucose in 0.1 M NaOH electrolyte solution. The amperometric technique has been used to investigate the concentrations of glucose in blood serum samples at different time intervals.

The amperometric response of the samples shows a continuous increase in current signal upon the addition of diluted blood serum. After recording the current, the glucose concentrations of the diluted samples are determined with the help of amperometric current and the linear equation and then the actual concentrations of glucose are calculated. The amperometric responses of the four samples are presented in Fig. S5 (ESI†).

The recoveries of the glucose concentration in four different biological samples are recorded in Table 1. It can clearly be seen that the recovery of sample solutions with various glucose concentrations appears to be in between 96 and 99% with a less relative standard deviation. The results (Table 1) are in good agreement with those detected and measured using the MISPA NEO Biochemistry Analyzer system in the hospital. Thus, the biosensor can be utilized as an alternate way to detect and quantify glucose in serum samples.

3.3. Protein adsorption study

The interaction of proteins with material surfaces has garnered unperturbed attention due to its relevance in biomedical device engineering and biotechnology. A detailed understanding of

Table 1 The recovery results for the determination of glucose in human blood serum samples

Sample no.	Reported (mM)	Found (mM)		Recovery (%)	RSD[a]
		Diluted	Calculated		
S1	4.9	0.485	4.85	99.0	3.2
S2	1.92	0.189	1.89	98.4	2.8
S3	4.85	0.474	4.74	97.7	3.1
S4	5.1	0.489	4.89	95.8	3.2

[a] RSD (%) was calculated from three repetitive measurements.

the protein–surface interactions is of utmost importance for designing the surfaces of biosensors and bioassays.[46,62] Proteins readily get adsorbed onto available solid surfaces; but this adsorption often causes conformational changes of proteins which can lead to functional inactivation and formation of a gel-like layer of the denatured proteins.[63,64] The layer of the denatured proteins inhibits the proper action of bio and immunosensors by fibrous encapsulation and membrane biodegradation that ultimately result in failure of the sensor *in vivo*. Therefore, study of protein adsorption along with the conformational change can deliver relevant information regarding the effectiveness of the sensor in real sample application. To determine the signature of protein adsorption onto the surface of Cu_2O octahedrons, at the start, a calibration curve has been developed by monitoring the intrinsic fluorescence maxima of the respective proteins using their known concentrations (Fig. S6, ESI†). The residual protein concentrations in the supernatant after adsorption of proteins are measured by the fluorescence intensity of the same and with the aid of the calibration curve. The amount of proteins adsorbed on the material surface is listed in Table 2. Fibrinogen is found to have the most affinity towards the Cu_2O surface, while hemoglobin is found to have the least.

CD spectra can indicate whether the proteins are in the adsorbed or desorbed state or in the hard or soft corona region, by observing the minimal structural alterations of proteins near the microstructure surfaces, and choosing definite buffer medium serves a vital role in the final conclusion.[65,66] Due to stronger ionic interaction in phosphate buffer (used in this study), microstructure surfaces are usually observed to adsorb more proteins than other buffer media like glycine.[67] Structural studies of the proteins in the supernatant solution hold great prominence and the reason is twofold. Primarily, it is well known that adsorption of protein is a dynamic procedure and the adsorbed protein molecules undergo exchange with the bare ones in solution continuously. The ordered structure of the studied proteins may vary through the course of the process. CD spectra of the supernatant solution have the ability to provide significant information in relation to the resultant structure of the concerned proteins as the outcome of the dynamic adsorption and desorption processes.[68] To the best of our knowledge, the interaction between the Cu_2O octahedrons and the studied four proteins has not disclosed previously. CD spectra of the proteins indicate a trivial change in the helicity (Table ST2, ESI†) and further confirm the low protein adsorption. The changes in the secondary and tertiary structures of the selected proteins indicate very weak interactions. Fig. S7(a–d) (ESI†) represents the change of CD spectrum for the concerned proteins (a: HSA, b: Fib, c: Hb, and d: γ-GB) and the results clearly indicate a decrease in the helicity of the α-helix of the respective proteins compared to their native state due to interaction.

Secondarily, the electrostatic interaction parameters are very crucial before applying the microstructures in real system analysis. DLS and zeta potential studies have also been implemented to understand the phenomenon. Zeta potential measurement gives additional insights into the protein adsorption and the data with regard to the surface charge of the native proteins, proteins present in the supernatant and adsorbed on the Cu_2O octahedrons are given in Table 2.

As far as the stability of the protein is concerned, DLS study yielded no size alteration of the studied proteins after incubation. This was an initial indication of the weak interaction amongst the proteins and the octahedrons. The reported hydrodynamic radii of the proteins in the native form presented here are in coherence with those reported previously.[69,70] The size distribution of the Cu_2O octahedrons before and after protein adsorption, (Fig. S8 and S9, ESI†) also convey that the synthesized microstructures have not shown aggregation in the biological fluid environment. However, the surface of the microstructures does not appear to be smooth anymore after protein adsorption (Fig. S10, ESI†) which is an indication towards the noisy data of the Cu_2O modified electrode in real human serum samples.

Zeta potential (ζ) measurement is a useful technique to realize the state of protein during adsorption and changes in the orientation on the surface of particles. The proteins in their native state disclose negative ζ values and on measuring the Cu_2O octahedrons, they display negative ζ values as well. Initial

Table 2 Hydrodynamic radius and zeta potential data of the proteins in the native state, in the supernatant and at the Cu_2O surface and the amount of protein adsorbed

System	Hydrodynamic radius (nm)		Zeta potential (mV)			Amount of protein adsorbed (mg g^{-1})
	Native	Supernatant	Native	Supernatant	At Cu_2O surface	
Fib	10.17 ± 0.2	—	−9.73 ± 1.67	—	—	98.33
Fib_Cu_2O	—	10.45 ± 0.3	—	−10.21 ± 2.04	−21.63 ± 2.67	
Hb	3.06 ± 0.16	—	−7.23 ± 1.48	—	—	36.82
Hb_Cu_2O	—	3.13 ± 0.31	—	−6.72 ± 1.56	−37.42 ± 3.79	
γ-GB	5.42 ± 0.25	—	−10.60 ± 1.36	—	—	55.12
γ-GB_Cu_2O	—	6.08 ± 0.33	—	−8.54 ± 1.78	−32.37 ± 3.15	
HSA	3.43 ± 0.21	—	−12.10 ± 2.13	—	—	64.73
HSA_Cu_2O	—	3.56 ± 0.28	—	−10.15 ± 2.12	−31.55 ± 2.12	

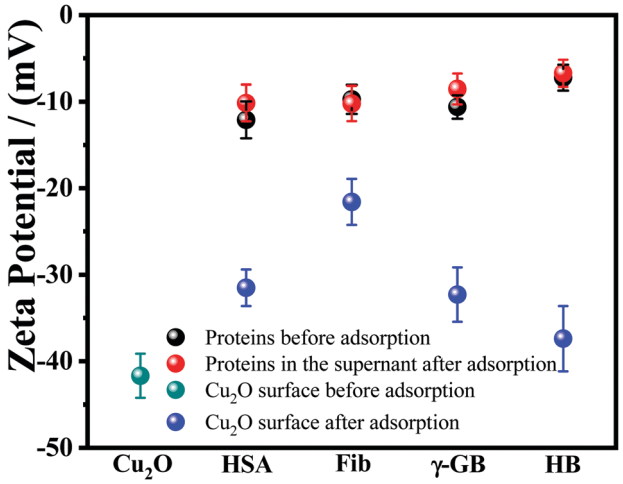

Fig. 5 Zeta potentials of the octahedrons in the absence and presence of proteins and for the proteins in the native state and in the supernatant.

ζ measurement of the Cu_2O microstructures as well as the native proteins in buffer pH ~ 7.2 divulge negative surface charges in all of them. There has been very little change in the surface charge of proteins present in the supernatant after adsorption. The effect of protein adsorption on the surface charge of Cu_2O octahedrons has also been examined by ζ measurement. The zeta potentials of the microstructures before and after adsorption are shown in Fig. 5. Protein adsorption decreases the surface charge of the Cu_2O octahedrons, and the value is dependent on the amount of protein adsorbed on the materials. The data are listed in Table 2. The amount of diminution of surface charge is found to be the maximum in the case of fibrinogen whereas hemoglobin is the minimum in this case. The specific electrostatic interaction and non-specific attraction between the negatively charged Cu_2O octahedrons and positively charged small pockets of proteins can be held responsible for adsorption. Although the global net charge of the proteins has negative values at pH ~ 7.2 (Table 2), the net charges of different domains and subdomains are different. In the case of fibrinogen, we presume that the positively charged αC domain interacts with the Cu_2O surface rather than the negatively charged E and D subdomains.[68] The minor positive regions in other proteins may not be totally accessible for interaction and thus, for HSA, Hb and γ-GB the adsorption is very low compared to those reported in other studies.[71–73] Accordingly, the conformations of the adsorbed proteins are quite similar to their respective native state and the loss of α-helix can be attributed to the continuous dynamic exchange process. Therefore, the weak adsorption and interaction can be attributed to the weak electrostatic interaction due to the negative surface charge on both the materials.[71–74]

Conclusions

In conclusion, we have successfully designed and developed fine quality uniform Cu_2O octahedrons with a "clean surface" in gram scale utilizing PVP-10k as the capping agent to tailor the shape at a low temperature. Cyclic voltammetry and amperometric techniques have been employed to assess the electrocatalytic properties of the Cu_2O octahedron modified electrode towards glucose electro-oxidation in alkaline media. The low-cost biosensor exhibits excellent performance towards selectivity, sensitivity, stability, reproducibility and wide linear range. Furthermore, this work advances the application of the electrochemical biosensor for the rapid, sensitive and highly selective detection of glucose in real samples with decent repeatability. The analytical performance of the biosensor is analogous to the conventional methods and encompasses a full range of clinically relevant concentrations of glucose in whole blood. An unprecedented adsorption analysis involving the devised biosensor and common blood proteins (HSA, Fib, Hb and γ-GB) is accomplished using DLS, zeta potential, steady state fluorescence and CD measurements. The results propose reduced protein adsorption on the Cu_2O octahedron surface mostly due to the electrostatic interaction. We sincerely believe the present study holds great potential for contriving a more sophisticated and miniature molecular level device with miscellaneous functions involving pure oxides. Further work is in progress to improve the sensitivity and stability of Cu_2O biosensors for practical biological applications and clinical detection.

Ethical statement

The serum samples were a gift by Serobacto Pathological Laboratory for academic purposes only. All the experiments were performed in compliance with relevant laws or guidelines of UGC (UGC 2017a, The UGC Research Development and Innovation Programs Implementation Guidelines 2017, Web 22) and approved by the Institutional Research Ethics Committee, Jadavpur University (Registration Number: 1805/GO/Re/S/15/CPCSEA), Kolkata, India. Study participants were fully informed regarding the purposes of the study and consent was obtained.

Conflicts of interest

The authors declare that they have no conflict of interest.

Acknowledgements

S. R. and S. C. B. thank the Department of Science & Technology, New Delhi, Government of India (DST-SERB Grant No. EMR/2015/000678/IPC) for financial support. R. R. acknowledges UGC, New Delhi, Government of India (No. F.30-509/2020(BSR)) for financial assistance. The authors are very grateful to Dr Hrishikesh Mishra, Serobacto Pathological Laboratory for providing the serum samples with standard values.

References

1 D. W. Hwang, S. Lee, M. Seo and T. D. Chung, *Anal. Chim. Acta*, 2018, **1033**, 1–34.
2 E. W. Nery, M. Kundys, P. S. Jeleń and M. Jönsson-Niedziólka, *Anal. Chem.*, 2016, **88**, 11271–11282.

3 A. Heller and B. Feldman, *Chem. Rev.*, 2008, **108**, 2482–2505.
4 X. Niu, X. Li, J. Pan, Y. He, F. Qiu and Y. Yan, *RSC Adv.*, 2016, **6**, 84893–84905.
5 N. P. Shetti, S. D. Bukkitgar, K. R. Reddy, C. V. Reddy and T. M. Aminabhavi, *Biosens. Bioelectron.*, 2019, **141**, 111417.
6 J. Wang, *Chem. Rev.*, 2008, **108**, 814–825.
7 H. Lee, Y. J. Hong, S. Baik, T. Hyeon and D. H. Kim, *Adv. Healthcare Mater.*, 2018, **7**, 1–14.
8 C. Sabu, T. K. Henna, V. R. Raphey, K. P. Nivitha and K. Pramod, *Biosens. Bioelectron.*, 2019, **141**, 111201.
9 G. Gnana Kumar, G. Amala and S. M. Gowtham, *RSC Adv.*, 2017, **7**, 36949–36976.
10 H. Zhu, L. Li, W. Zhou, Z. Shao and X. Chen, *J. Mater. Chem. B*, 2016, **4**, 7333–7349.
11 J. L. Lin and J. P. Wolfe, *Phys. Rev. Lett.*, 1993, **71**, 1222–1225.
12 D. Snoke, *Science*, 2002, **298**, 1368–1372.
13 W. Yu, F. Li, H. Wang, E. Alarousu, Y. Chen, B. Lin, L. Wang, M. N. Hedhili, Y. Li, K. Wu, X. Wang, O. F. Mohammed and T. Wu, *Nanoscale*, 2016, **8**, 6173–6179.
14 R. Wick and S. D. Tilley, *J. Phys. Chem. C*, 2015, **119**, 26243–26257.
15 C. Y. Chu and M. H. Huang, *J. Mater. Chem. A*, 2017, **5**, 15116–15123.
16 X. Wan, J. Wang, L. Zhu and J. Tang, *J. Mater. Chem. A*, 2014, **2**, 13641–13647.
17 Z. Gao, J. Liu, J. Chang, D. Wu, J. He, K. Wang, F. Xu and K. Jiang, *CrystEngComm*, 2012, **14**, 6639–6646.
18 X. Liu, Y. Sui, X. Yang, L. Jiang, F. Wang, Y. Wei and B. Zou, *RSC Adv.*, 2015, **5**, 59099–59105.
19 K. Chanda, S. Rej and M. H. Huang, *Nanoscale*, 2013, **5**, 12494–12501.
20 Y. H. Tsai, K. Chanda, Y. T. Chu, C. Y. Chiu and M. H. Huang, *Nanoscale*, 2014, **6**, 8704–8709.
21 Y. Kwon, A. Soon, H. Han and H. Lee, *J. Mater. Chem. A*, 2015, **3**, 156–162.
22 Y. Guo, H. Lei, L. Xiong, B. Li, Z. Chen, J. Wen, G. Yang, G. Li and G. Fang, *J. Mater. Chem. A*, 2017, **5**, 11055–11062.
23 J. Lv, C. Kong, X. Hu, X. Zhang, K. Liu, S. Yang, J. Bi, X. Liu, G. Meng, J. Li, Z. Yang and S. Yang, *J. Mater. Chem. B*, 2017, **5**, 8686–8694.
24 W. Liu, G. Chai, J. Zhang, M. Wang, Y. Dai and Q. Yang, *New J. Chem.*, 2020, **44**, 15662–15670.
25 Y. Wang, Z. Ji, X. Shen, G. Zhu, J. Wang and X. Yue, *New J. Chem.*, 2017, **41**, 9223–9229.
26 H. C. Chen, W. R. Su and Y. C. Yeh, *ACS Appl. Mater. Interfaces*, 2020, **12**, 32905–32914.
27 M. Waqas, L. Wu, H. Tang, C. Liu, Y. Fan, Z. Jiang, X. Wang, J. Zhong and W. Chen, *ACS Appl. Nano Mater.*, 2020, **3**, 4788–4798.
28 S. D. Rani, R. Ramachandran, S. Sheet, M. A. Aziz, Y. S. Lee, A. G. Al-Sehemi, M. Pannipara, Y. Xia, S. Y. Tsai, F. L. Ng, S. M. Phang and G. G. Kumar, *Sens. Actuators, B*, 2020, **312**, 127886.
29 Z. C. Zhang, B. Xu and X. Wang, *Chem. Soc. Rev.*, 2014, **43**, 7870–7886.
30 Z. Fan and H. Zhang, *Chem. Soc. Rev.*, 2016, **45**, 63–82.
31 S. Rakshit, S. P. Moulik and S. C. Bhattacharya, *J. Phys. Chem. B*, 2015, **119**, 8457–8467.
32 S. Rakshit, S. Chall, S. S. Mati, A. Roychowdhury, S. P. Moulik and S. C. Bhattacharya, *RSC Adv.*, 2013, **3**, 6106–6116.
33 S. Chall, S. S. Mati, S. Rakshit and S. C. Bhattacharya, *J. Phys. Chem. C*, 2013, **117**, 25146–25159.
34 S. Sun and Z. Yang, *RSC Adv.*, 2014, **4**, 3804–3822.
35 S. Rakshit, S. Ghosh, S. Chall, S. S. Mati, S. P. Moulik and S. C. Bhattacharya, *RSC Adv.*, 2013, **3**, 19348–19356.
36 K. M. Koczkur, S. Mourdikoudis, L. Polavarapu and S. E. Skrabalak, *Dalton Trans.*, 2015, **44**, 17883–17905.
37 L. Liu, W. Yang, Q. Li, S. Gao and J. K. S. Shang, *ACS Appl. Mater. Interfaces*, 2014, **6**, 5629–5639.
38 Z. Cheng, J. Xu, H. Zhong, X. Chu and J. Song, *Mater. Lett.*, 2011, **65**, 1871–1874.
39 J. C. Park, J. Kim, H. Kwon and H. Song, *Adv. Mater.*, 2009, **21**, 803–807.
40 R. Chen and J. E. Riviere, *Biological surface adsorption index of nanomaterials: Modelling surface interactions of nanomaterials with biomolecules*, 2017, vol. 947.
41 C. Lim, S. Slack, S. Ufer and E. Lindner, *Pure Appl. Chem.*, 2004, **76**, 753–764.
42 J. J. Gooding, *Nat. Nanotechnol.*, 2019, **14**, 1089–1090.
43 N. Arroyo-Currás, J. Somerson, P. A. Vieira, K. L. Ploense, T. E. Kippin and K. W. Plaxco, *Proc. Natl. Acad. Sci. U. S. A.*, 2017, **114**, 645–650.
44 J. E. Contreras-Naranjo and O. Aguilar, *Biosensors*, 2019, **9**, 1–23.
45 S. A. Bhakta, E. Evans, T. E. Benavidez and C. D. Garcia, *Anal. Chim. Acta*, 2015, **872**, 7–25.
46 R. Ziółkowski, A. Kaczmarek, I. Kośnik and E. Malinowska, *Bioelectrochemistry*, 2020, **132**, 107415.
47 U. Sakulkhu, M. Mahmoudi, L. Maurizi, G. Coullerez, M. Hofmann-Amtenbrink, M. Vries, M. Motazacker, F. Rezaee and H. Hofmann, *Biomater. Sci.*, 2015, **3**, 265–278.
48 X. R. Xia, N. A. Monteiro-Riviere, S. Mathur, X. Song, L. Xiao, S. J. Oldenberg, B. Fadeel and J. E. Riviere, *ACS Nano*, 2011, **5**, 9074–9081.
49 Y. Sui, W. Fu, H. Yang, Y. Zeng, Y. Zhang, Q. Zhao, Y. Li, X. Zhou, Y. Leng, M. Li and G. Zou, *Cryst. Growth Des.*, 2010, **10**, 99–108.
50 Y. Shang and L. Guo, *Adv. Sci.*, 2015, **2**, 1500140.
51 P. Lignier, R. Bellabarba and R. P. Tooze, *Chem. Soc. Rev.*, 2012, **41**, 1708–1720.
52 S. Sun, X. Zhang, Y. Sun, J. Zhang, S. Yang, X. Song and Z. Yang, *ACS Appl. Mater. Interfaces*, 2013, **5**, 4429–4437.
53 H. Ren, X. Zhang, X. Zhang, J. Cui, Q. Yang, C. Kong, Z. Yang and S. Sun, *CrystEngComm*, 2020, **22**, 2042–2048.
54 J. He, Y. Jiang, J. Peng, C. Li, B. Yan and X. Wang, *J. Mater. Sci.*, 2016, **51**, 9696–9704.
55 P. Kannan, T. Maiyalagan, E. Marsili, S. Ghosh, J. Niedziolka-Jönsson and M. Jönsson-Niedziolka, *Nanoscale*, 2016, **8**, 843–855.
56 P. Kannan, T. Maiyalagan, E. Marsili, S. Ghosh, L. Guo, Y. Huang, J. A. Rather, D. Thiruppathi, J. Niedziolka-

Jönsson and M. Jönsson-Niedziolka, *Analyst*, 2017, **142**, 4299–4307.
57 J. Tashkhourian, S. F. Nami-Ana and M. Shamsipur, *Anal. Chim. Acta*, 2018, **1034**, 63–73.
58 L. N. Wu, J. P. Zhong, M. Waqas, Z. Jiang, Y. J. Fan, Y. Sun, J. Li and W. Chen, *Electrochim. Acta*, 2019, **318**, 837–846.
59 J. N. Tiwari, V. Vij, K. C. Kemp and K. S. Kim, *ACS Nano*, 2016, **10**, 46–80.
60 W. Zhao, R. Zhang, S. Xu, J. Cai, X. Zhu, Y. Zhu, W. Wei, X. Liu and J. Luo, *Biosens. Bioelectron.*, 2018, **100**, 497–503.
61 H. Zhang, Y. Yu, X. Shen and X. Hu, *New J. Chem.*, 2020, **44**, 1993–2000.
62 R. A. Latour, *Colloids Surf., B*, 2020, **191**, 110992.
63 S. H. De Paoli Lacerda, J. J. Park, C. Meuse, D. Pristinski, M. L. Becker, A. Karim and J. F. Douglas, *ACS Nano*, 2010, **4**, 365–379.
64 S. Pramanik, P. Banerjee, A. Sarkar and S. C. Bhattacharya, *J. Lumin.*, 2008, **128**, 1969–1974.
65 A. Salis, L. Cappai, C. Carucci, D. F. Parsons and M. Monduzzi, *J. Phys. Chem. Lett.*, 2020, **11**, 6805–6811.
66 S. Brudar and B. Hribar-Lee, *Biomolecules*, 2019, **9**, 65.
67 Z. Adamczyk, A. Pomorska, M. Nattich-Rak, M. Wytrwal-Sarna and A. Bernasik, *J. Colloid Interface Sci.*, 2018, **530**, 631–641.
68 Y. Chen, X. Zhang, Y. Gong, N. Zhao, T. Zeng and X. Song, *J. Colloid Interface Sci.*, 1999, **214**, 38–45.
69 J. K. Armstrong, R. B. Wenby, H. J. Meiselman and T. C. Fisher, *Biophys. J.*, 2004, **87**, 4259–4270.
70 M. Nag, D. Das, D. Bandyopadhyay and S. Basak, *Phys. Chem. Chem. Phys.*, 2015, **17**, 19139–19148.
71 M. E. Soderquist and A. G. Walton, *J. Colloid Interface Sci.*, 1980, **75**, 386–397.
72 M. Karavitis, C. Fronticelli, W. S. Brinigar, G. B. Vasquez, V. Militello, M. Leone and A. Cupane, *J. Biol. Chem.*, 1998, **273**, 23740–23749.
73 E. Topoglidis, C. J. Campbell, A. E. G. Cass and J. R. Durrant, *Langmuir*, 2001, **17**, 7899–7906.
74 P. Bolel, S. Datta, N. Mahapatra and M. Halder, *J. Phys. Chem. B*, 2014, **118**, 26–36.

